Optics Letters

Ultra high power (100 kW) fiber laser welding of steel

Yousuke Kawahito,[1,2] Hongze Wang,[1,*] Seiji Katayama,[3] and Daichi Sumimori[3]

[1]Joining and Welding Research Institute (JWRI), Osaka University, 11-1 Mihogaoka, Ibaraki, Osaka 567-0047, Japan
[2]Japan Agency for Marine-Earth Science and Technology (JAMSTEC), 2-15 Natsushimacho, Yokosuka, Kanagawa Prefecture 237-0061, Japan
[3]Nadex Laser R&D Center, NADEX Co., Ltd., 62-31-2 Azono, Tsuruga, Fukui 914-0141, Japan
*Corresponding author: wanghz@jwri.osaka-u.ac.jp

Received 30 July 2018; revised 30 August 2018; accepted 31 August 2018; posted 4 September 2018 (Doc. ID 340778); published 21 September 2018

A 100 kW fiber laser was first used to weld steel. Speeds at the range between 0.3 and 5.0 m/min were tested, and the maximum weld bead depth of 70 mm was achieved by single pass welding. Solidification cracking and porosity occurred when the welding speed was lower than 0.5 m/min, while undercut appeared when the welding speed was higher than 3.0 m/min. Both the ratio of depth to width and the cross section area of the weld bead had a positively linear relationship with the welding speed. A high speed camera was used to observe the characteristics of the keyhole and molten pool. The average number of spatters increased with the welding speed, while the keyhole diameter and the length of the molten pool in front of the keyhole decreased with the welding speed. This Letter validates the application potential of a 100 kW ultra high power fiber laser in manufacturing, e.g., welding, cutting, and additive manufacturing.

OCIS codes: (350.3390) Laser materials processing; (140.0140) Lasers and laser optics.

https://doi.org/10.1364/OL.43.004667

Since being first developed, to the best of our knowledge, in the early 1960s, the laser has been widely used in manufacturing [1–4] because of the ability to melt the material instantaneously. Various laser systems have been developed, and their applications have been investigated [5–8]. These laser systems achieve wide applications in welding [9], cutting [10], heat treatment [11], and additive manufacturing [12,13].

A thick steel sheet has been widely used in the shipping industry to bear the weight and ensure safety performance. Ship manufacturing puts forward a big challenge for the welding technique. The high power laser provides an effective solution for single pass welding of thick sheets, which have been widely used in industry. Various researchers have focused on this topic [8,14,15]. Zhang [15] adopted the 10 kW fiber laser in welding of 12 mm thick stainless steel, and the optimized parameters were achieved. Kawahito [14] adopted the 10 kW fiber laser in welding of 12 mm metallic glass successfully. Sokolov [16] adopted the fiber laser with the maximum power of 30 kW in welding, and the maximum weld bead depth of 25 mm was achieved, which is also the reported maximum power at present. However, laser welding of much thicker steel sheets with the single pass mode has rarely been reported because of the limitation in laser power. Though the vacuum laser welding method has been reported in welding of steel sheets with the thickness up to 75 mm [17], the application of this method is limited due to high airtightness requirements for the vacuum chamber. The multiple passes laser welding method has also been reported in welding of a steel sheet with the thickness up to 50 mm [18,19]. However, this method has low production efficiency because of the multiple welding passes, and defects may appear at the interface between two passes.

Recently, a continuous-wave 100 kW ytterbium fiber laser has been developed [20]. However, the potential of this ultra high power laser for welding application has rarely been reported. Exploring the ability of ultra high power lasers in manufacturing could broaden the application of the laser. In this Letter, the weldability of a 100 kW ytterbium fiber laser for steel was investigated. Characteristics of the weld bead were analyzed with the metallography experiment, and a high speed camera was used to observe the keyhole, molten pool, and spatters. This Letter validates the application potential of a 100 kW ultra high power fiber laser in manufacturing.

A continuous-wave ytterbium fiber laser oscillator with a maximum power of 100 kW developed by IPG Laser GmbH [20] was used as the heat source for welding in this Letter. The beam is delivered through an optical fiber of 0.5 mm in diameter and 50 m in length, and the beam parameter product (BPP) is 25.0 mm * mrd. The focusing feature and beam profile are shown in Fig. 1. Figure 1(a) shows the focusing feature, where the diameter of the laser beam at the focus position is 1.0 mm, which is obviously larger than that of the conventional laser beam with lower power [21]. Figure 1(b) shows the beam profile at the focus position, where the laser energy is generally uniformly distributed on the cross section, and the wall of the beam profile is steep, which indicates good beam quality.

In the experiment, the laser power was set to be 100 kW, the focus position of the laser beam was set on the upper surface of the stainless steel (SUS304) sheet with the thickness of 90 mm, and the welding speed within the range between 0.3 and

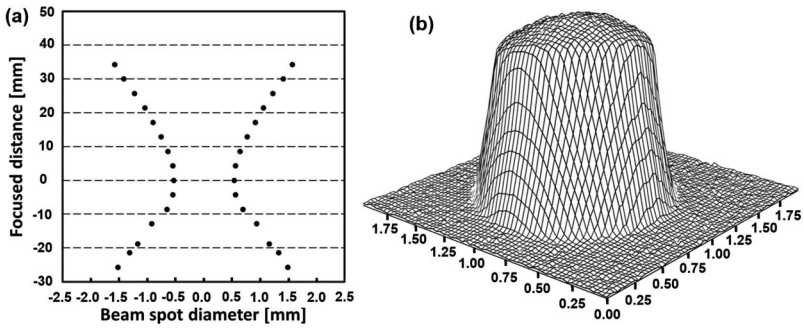

Fig. 1. Schematic of 100 kW fiber laser beam: (a) laser beam diameter at different focused distances; (b) beam profile at the focused position.

5.0 m/min was used. The focus distance of this laser system is 1000 mm. The laser head was inclined with the angle of 10°, and N_2 was used as the shielding gas to prevent the oxidation of the molten pool. Figure 2(a) shows the characteristics of weld bead surface and cross section at different welding speeds. Figure 2(b) shows the measured weld bead depth at different welding speeds. For each speed, three cross sections at the random position were prepared, and their weld bead depths and widths on the upper surface were measured. The average of these three measured depths was used to represent the depth at this welding parameter, and the average of the measured widths was used to represent the width. As shown, the weld bead depth decreased with the increased welding speed, and the maximum depth of 70 mm appeared at the speed of 0.3 mm. To the best of our knowledge, this is the reported maximum weld bead depth in laser single pass welding of steel. When the welding speed was lower than or equal to 0.5 m/min, there were porosities or cracks in the cross section of the weld bead. When the welding speed was higher than or equal to 3.0 m/min, there were undercut defects. The speed window for high quality weld bead was between 1.0 and 2.0 m/min.

Figure 2(c) shows the effects of welding speed on the ratio of weld bead depth to width. The slope of the fitted line b is 1.31, the intercept a is 1.37, and the coefficient of determination R-squared R^2 is 0.91, which indicates that a good positive linear relationship exists between the ratio and welding speed. The ratio of weld depth to width could act as an indicator for energy efficiency. The larger ratio means that much more energy could be used to penetrate into the material. Figure 2(d) shows the relationship between the cross section area of the weld bead and line energy of the laser beam. The line energy was defined to be the ratio between laser power and welding speed with the unit of kilojoules per millimeter (kJ/mm). The slope of fitted line b is 5.4, intercept a is 50.6, and the coefficient of determination R-squared R^2 is 1.0, which indicates that a perfect positive linear relationship exists between the weld bead area and line energy.

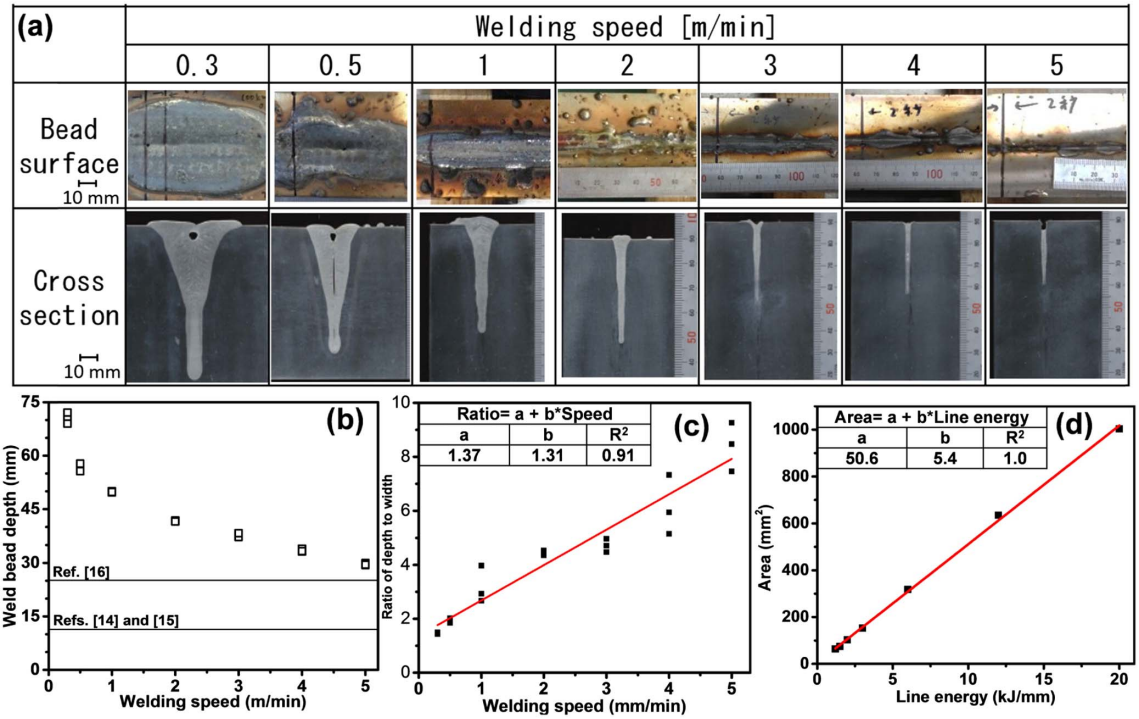

Fig. 2. Effects of welding speed on (a) characteristics of the upper surface and cross section, (b) weld bead depth, (c) ratio of weld bead depth to width, and (d) relationship between weld bead area and line energy.

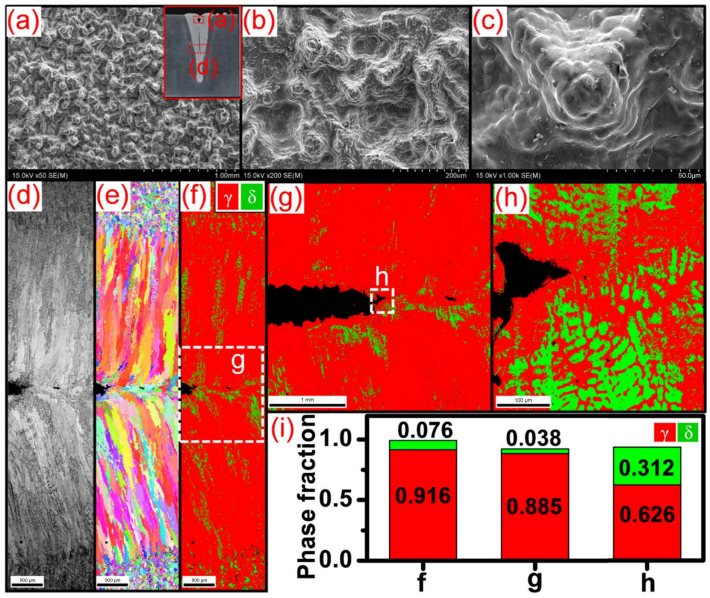

Fig. 3. Typical characteristics of porosity and crack in the weld bead at the welding speed of 0.5 m/min: (a) to (c) represent the microstructure in the porosity with the magnification values of 50, 200. and 1000, respectively; (d) represents the micro-characteristics of the local zone in the weld bead with crack observed by SEM; (e) and (f) represent grain orientation and phase distribution in (e) observed by EBSD, respectively; (g) represents the enlarged view of zone (g) in (f); (h) represents the enlarged view of zone (h) in (g); (i) shows the comparison of phase distribution among (f), (g), and (h).

Figure 3 shows the typical characteristics of porosity and crack in the weld bead at the welding speed of 0.5 m/min. Figures 3(a)–3(c) represent the microstructure in the porosity with the magnification values of 50, 200, and 1000, respectively. The position of the porosity is shown in zone (a) of the weld bead in the top right-hand corner of Fig. 3(a).

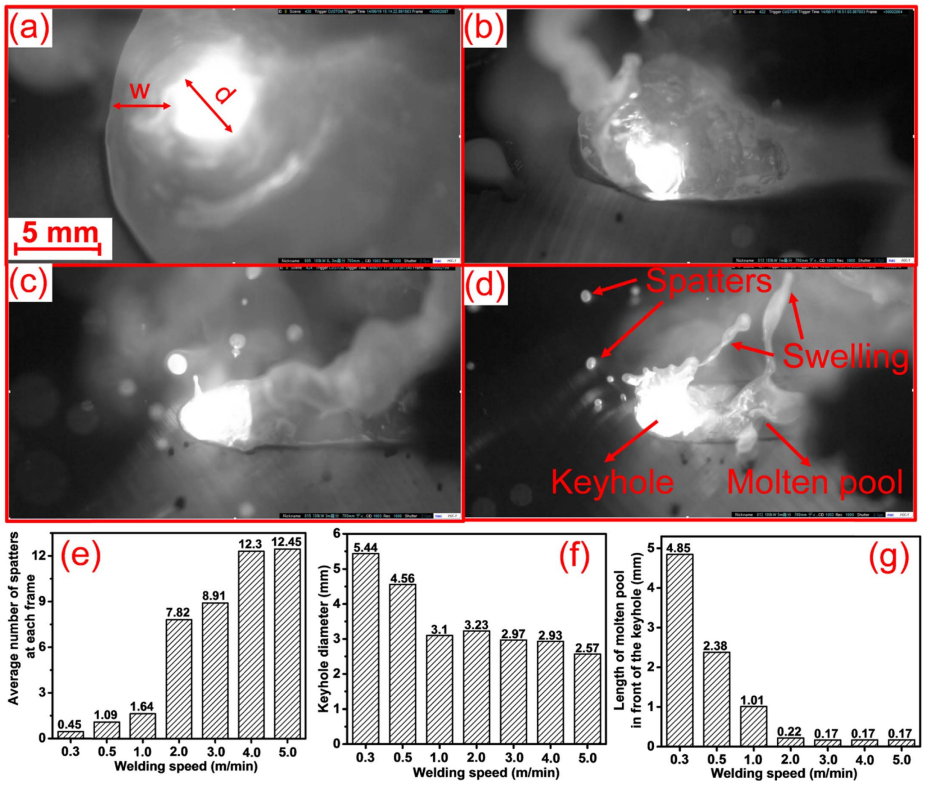

Fig. 4. Characteristics of the keyhole and molten pool observed by high speed camera: (a) to (d) represent the characteristics observed by a high speed camera at the welding speeds of 0.3, 1.0, 3.0, and 5.0 m/min, respectively; (d) represents the average spatter number at each frame; (f) represents the keyhole diameter; and (g) represents the length of the molten pool in front of the keyhole. (See Visualization 1, Visualization 2, Visualization 3, and Visualization 4.)

As shown, many dendritic crystals were observed, which validated the appearance of solidification porosity. Figures 3(d) and 3(e) show the microstructure observed by a scanning electron microscope (SEM) and the grain orientation observed by electron backscatter diffraction (EBSD), respectively. The position of this picture is shown in zone (d) of the weld bead in the top right-hand corner of Fig. 3(a). Tiny equiaxed grain was observed in the base metal zone, while coarse columnar grain was observed in the weld bead zone. The solidification crack appeared in the middle of the weld bead. Figures 3(f)–3(h) show the phase distribution observed by EBSD. The steel mainly consists of the γ phase and δ phase, while the ratio of these two phases varies with location. As shown, the largest ratio of the γ phase appears in Fig. 3(f), while the lowest ratio of the γ phase appears in Fig. 3(h). It seems that the ratio of the δ phase increases significantly in the zone adjacent to the crack.

Figure 4 shows the characteristics of the keyhole and molten pool observed by a high speed camera. Figures 4(a)–4(d) represent the characteristics of the upper surface observed by a high speed camera at the welding speeds of 0.3, 1.0, 3.0, and 5.0, respectively. The characteristics of the keyhole and molten pool vary with the welding speed. Figure 4(e) shows the effect of the welding speed on the average number of spatters at each frame of the picture captured by a high speed camera. To count the number of spatters, twenty pictures were collected randomly from the video, and the average number of the spatters at each frame of the picture was calculated. As shown, the average number of spatters increases with the welding speed. When the welding speed is slower than 2.0 m/min, the number of spatters is less than 2.0, which is a relatively low level. The number of spatters increases significantly when the welding speed is faster than 2.0 m/min, and the average number of spatters reaches 12.45 at the welding speed of 5.0 m/min. These observed experiment results of the spatters during laser welding from a high speed video are consistent with the spatters on the surface of the weld bead. With the increase of welding speed, the instability of the keyhole and molten pool increase, which leads to the increase in the number of spatters. The diameter of the keyhole and the length of the molten pool in front of the keyhole were also measured from the high speed camera. The average of the measured values from three pictures at random times was calculated. Figure 4(f) shows the effect of welding speed on the diameter of the keyhole. The measured keyhole diameter decreases with the increase of welding speed. The keyhole diameter is 5.44 mm at the welding speed of 0.3 m/min, while it decreases to 2.57 mm at the welding speed of 5.0 m/min. Figure 4(g) shows the effect of welding speed on the length of the molten pool in front of the keyhole. The measured length also decreases with the increase of welding speed. The length is 4.85 mm at the welding speed of 0.3 m/min, while it decreases to 0.17 mm at the welding speed of 5.0 m/min. The heat is accumulated in the molten pool at the low welding speed situation, which leads to the increase in sizes of the keyhole and molten pool.

To sum up, the performance of the 100 kW laser for welding extra thick SUS304 steel with the velocity between 0.3 and 5.0 m/min was tested. The maximum penetration depth of 75 mm was first, to the best of our knowledge, achieved by single pass laser welding. The cross section area of the weld bead was positively and linearly related to the line energy of the laser beam. With the increase of welding speed from 0.3 to 5.0 m/min, the ratio of weld depth to width increased from 1.5 to 8.4. The number of spatters increased from 0.45 at 0.3 m/min to 12.45 at 5.0 m/min. The length of the molten pool in front of the keyhole decreases from 4.85 mm at 0.3 m/min to 0.17 mm at 5.0 m/min. This Letter validates the application potential of the 100 kW ultra high power fiber laser in single pass welding of a thick sheet.

Funding. Grant-in-Aid for Scientific Research (17K06818).

REFERENCES

1. S. David and T. DebRoy, Science **257**, 497 (1992).
2. T. DebRoy, H. Wei, J. Zuback, T. Mukherjee, J. Elmer, J. Milewski, A. Beese, A. Wilson-Heid, A. De, and W. Zhang, Prog. Mater. Sci. **92**, 112 (2017).
3. M. Gao, S. Mei, X. Li, and X. Zeng, Scr. Mater. **67**, 193 (2012).
4. M. Sieben and F. Brunnecker, Nat. Photonics **3**, 270 (2009).
5. H. Wang, Y. Kawahito, R. Yoshida, Y. Nakashima, and K. Shiokawa, Opt. Lett. **42**, 2251 (2017).
6. R. K. Huang, B. Samson, B. Chann, B. Lochman, and P. Tayebati, *High Power Diode Lasers and Systems Conference (HPD)* (IEEE, 2015), pp. 29–30.
7. A. Matsunawa, N. Seto, J.-D. Kim, M. Mizutani, and S. Katayama, *High-Power Lasers in Manufacturing* (International Society for Optics and Photonics, 2000), pp. 34–46.
8. Y. Kawahito, M. Mizutani, and S. Katayama, Sci. Tech. Weld. Join. **14**, 288 (2009).
9. Y. Kawahito and H. Wang, Scr. Mater. **154**, 73 (2018).
10. C. Chen, M. Gao, and X. Zeng, Int. J. Mach. Tools Manuf. **109**, 58 (2016).
11. Q. Meng, Y. Liu, H. Yang, and T.-H. Nam, Scr. Mater. **65**, 1109 (2011).
12. A. Plotkowski, O. Rios, N. Sridharan, Z. Sims, K. Unocic, R. Ott, R. Dehoff, and S. Babu, Acta Mater. **126**, 507 (2017).
13. Y. Lee, M. Nordin, S. Babu, and D. Farson, Weld. J. **93**, 292S (2014).
14. Y. Kawahito, T. Terajima, H. Kimura, T. Kuroda, K. Nakata, S. Katayama, and A. Inoue, Mater. Sci. Eng. B **148**, 105 (2008).
15. M. Zhang, G. Chen, Y. Zhou, and S. Liao, Mater. Des. **53**, 568 (2014).
16. M. Sokolov, A. Salminen, M. Kuznetsov, and I. Tsibulskiy, Mater. Des. **32**, 5127 (2011).
17. S. Katayama, Y. Abe, M. Mizutani, and Y. Kawahito, Trans. JWRI **40**, 15 (2011).
18. X. Zhang, E. Ashida, S. Tarasawa, Y. Anma, M. Okada, S. Katayama, and M. Mizutani, J. Laser Appl. **23**, 022002 (2011).
19. J. Feng, W. Guo, N. Irvine, and L. Li, Int. J. Adv. Manuf. Technol. **88**, 1821 (2017).
20. E. Shcherbakov, V. Fomin, A. Abramov, A. Ferin, D. Mochalov, and V. P. Gapontsev, *Advanced Solid State Lasers* (Optical Society of America, 2013), paper ATh4A. 2.
21. H. Wang, M. Nakanishi, and Y. Kawahito, J. Mater. Process. Technol. **249**, 193 (2017).